Bilayered smectic phase polymorphism in the dipolar Gay–Berne liquid crystal model

Mohammed Houssa, Luis F. Rull, and Jose M. Romero-Enrique

Citation: The Journal of Chemical Physics **130**, 154504 (2009); doi: 10.1063/1.3111953

View online: http://dx.doi.org/10.1063/1.3111953

View Table of Contents: http://scitation.aip.org/content/aip/journal/jcp/130/15?ver=pdfcov

Published by the AIP Publishing

Bilayered smectic phase polymorphism in the dipolar Gay–Berne liquid crystal model

Mohammed Houssa, Luis F. Rull, and Jose M. Romero-Enrique[a)]
Departamento de Física Atómica, Molecular y Nuclear, Area de Física Teórica, Universidad de Sevilla, Apartado de Correos 1065, 41080 Sevilla, Spain

(Received 10 November 2008; accepted 12 March 2009; published online 17 April 2009)

We present computer simulations of the Gay–Berne model with a strong terminal dipole. We report the existence of *different* stable antiferroelectric interdigitated bilayered phases in this model with diverse in-plane organization. The occurrence of these phases depends crucially on the value of the molecular elongation κ. For $\kappa=3$ we find an interdigitated bilayered smectic-A phase (absent when there is no dipole) and a bilayered smectic-T (or crystal) with positional in-plane tetragonal ordering, different from the hexatic observed in the absence of the molecular dipole. For $\kappa=4$, bilayered smectic-A and in-plane hexatic-ordered smectic-B (or crystal) phases are observed. © *2009 American Institute of Physics*. [DOI: 10.1063/1.3111953]

I. INTRODUCTION

Fluids presenting liquid-crystalline behavior are frequently constituted by molecules which possess strong dipolar groups. Indeed, one of the earliest attempts to explain the occurrence of liquid crystals by Born[1] attributed the mesophases to the presence of dipolar interactions. Although it is known that they are not essential in the formation of the ordered phases, the dipolar forces are shown to play an important role in their stabilization.[2–4] The examination of the effect of polar interactions on the structure and thermodynamic properties of fluids has been the subject of numerous studies. Most of the liquid crystal computer simulations with an embedded electric dipole has been performed by using the so-called Gay–Berne (GB) potential.[5] This model is the most widely studied with uniaxial anisotropy and attractive interactions.[6–13] Other models of dipolar mesogens, such as dipolar hard spherocylinders, have been also studied.[14–22] A good summary of theoretical and simulation studies of dipolar mesogens can be found in a paper by Varga *et al.*[23] The precise location and orientation of the dipole in the molecule are important in determining the structure of the liquid-crystalline phases. If we focus our attention to the case of the prolate GB molecules with the dipole located at the center of mass of the molecule and oriented along the molecular axis (central dipole), the dipolar interaction has a little effect on the isotropic-nematic transition but a marked stabilization of the positionally layered liquid-crystalline phases such the smectics has been seen. For oblate dipolar GB molecules, evidences of a ferroelectric nematic fluid have been observed.

A new phenomenology emerges when the dipole position shifts toward the end of the molecule. Experimentally different kinds of smectic phases have been observed when strong polar groups are present in the (rodlike) molecule: the usual monolayer SmA_1 phase, the bilayered SmA_2 phase (with a layer spacing equal to the length of the molecule), and SmA_d (which presents interdigitation between layers), among others.[24–26] These new smectic phases show antiferroelectric ordering, which may be modulated across each layer as in the Sm$\tilde{A}$ phase.[25]

From a theoretical and computer simulation point of view, the GB model with a terminal dipole has been studied by Berardi *et al.*[27–29] They carried out canonical ensemble Monte Carlo (NVTMC) computer simulations to study the influence of terminal dipoles in the phase diagram of the GB model, and they observed a stripped antiferroelectric bilayer structure with local ferroelectric order. More recently, they studied by NVTMC and variational theory the effect of the molecular dipole strength on the polymorphism of the smectic-A phase and a transition from noninterdigitated to interdigitated smectic-A molecular organization was observed.[29] This result contrasts with the observed for hard spherocylinders with a terminal dipole, in which a dramatic stabilization of the nematic phase relative to the smectic phase is reported.[17]

Almost all the studies carried out up to now focus on the layer organization (interdigitation, antiferroelectric ordering, etc.). However, these studies pay little attention to the way in which particles are organized on each layer. We will show by computer simulations that different layered phases are possible in the GB model with a strong terminal dipole. In addition to the SmA_d phase previously reported, we find two bilayered phases with in-plane positional ordering, being tetragonal for small elongations and hexatic for large elongations. The paper is organized as follows. Section II is devoted to present the model and details of the computer simulation methodology. In Sec. III we present our results for different elongations of the GB molecule, and we end up with our conclusions.

II. THE MODEL AND SIMULATION DETAILS

The dipolar GB intermolecular pair potential for prolate molecules consists of a short-ranged anisotropic contribution U_{ij}^{GB} and a long-ranged dipolar interaction U_{ij}^{dd}. The terminal

a)Electronic mail: enrome@us.es.

dipole is placed at a distance d from the center of mass of each molecule and parallel to the main axis of the molecule. The GB potential U_{ij}^{GB} has the following expression:[5]

$$U_{ij}^{\mathrm{GB}}(\mathbf{r}_{ij},\mathbf{u}_i,\mathbf{u}_j) = 4\varepsilon(\hat{\mathbf{r}}_{ij},\mathbf{u}_i,\mathbf{u}_j)[\rho_{ij}^{-12} - \rho_{ij}^{-6}], \tag{1}$$

where

$$\rho_{ij} = \frac{r_{ij} - \sigma(\hat{\mathbf{r}}_{ij},\mathbf{u}_i,\mathbf{u}_j) + \sigma_0}{\sigma_0}, \tag{2}$$

$\mathbf{u_i}$ is the unit vector along the symmetry axis of the molecule i, $r_{ij}=|\mathbf{r}_i-\mathbf{r}_j|$ is the distance along the intermolecular vector $\mathbf{r}_{ij}$ joining the centers of mass of the molecules, and $\hat{\mathbf{r}}_{ij}=\mathbf{r}_{ij}/r_{ij}$. The anisotropic contact distance $\sigma(\hat{\mathbf{r}}_{ij},\mathbf{u}_i,\mathbf{u}_j)$ and the depth of the interaction energy $\varepsilon(\hat{\mathbf{r}}_{ij},\mathbf{u}_i,\mathbf{u}_j)$ depend on the orientational unit vector, the length to breathe ratio ($\kappa=\sigma_{ee}/\sigma_{ss}$), and the energy depth anisotropy ($\kappa'=\epsilon_{ee}/\epsilon_{ss}$), which are defined as the ratio of the size and energy interaction parameters in the end-to-end (ee) and side-by-side (ss) configurations. Their expressions are given in terms of the length scale σ_0 and the energy unit ε_0 as

$$\frac{\sigma(\hat{\mathbf{r}}_{ij},\mathbf{u}_i,\mathbf{u}_j)}{\sigma_0} = \left[1 - \frac{\chi}{2}\left(\frac{(\hat{\mathbf{r}}_{ij}\cdot\mathbf{u}_i + \hat{\mathbf{r}}_{ij}\cdot\mathbf{u}_j)^2}{1+\chi(\mathbf{u}_i\cdot\mathbf{u}_j)} + \frac{(\hat{\mathbf{r}}_{ij}\cdot\mathbf{u}_i - \hat{\mathbf{r}}_{ij}\cdot\mathbf{u}_j)^2}{1-\chi(\mathbf{u}_i\cdot\mathbf{u}_j)}\right)\right]^{-1/2}, \tag{3}$$

$$\frac{\varepsilon(\hat{\mathbf{r}}_{ij},\mathbf{u}_i,\mathbf{u}_j)}{\epsilon_0} = [\epsilon_1(\mathbf{u}_i,\mathbf{u}_j)]^{\nu} \times [\epsilon_2(\hat{\mathbf{r}}_{ij},\mathbf{u}_i,\mathbf{u}_j)]^{\nu'}, \tag{4}$$

where

$$\epsilon_1(\mathbf{u}_i,\mathbf{u}_j) = [1-\chi^2(\mathbf{u}_i\cdot\mathbf{u}_j)^2]^{-1/2}, \tag{5}$$

$$\epsilon_2(\hat{\mathbf{r}}_{ij},\mathbf{u}_i,\mathbf{u}_j) = 1 - \frac{\chi'}{2}\left[\frac{(\hat{\mathbf{r}}_{ij}\cdot\mathbf{u}_i + \hat{\mathbf{r}}_{ij}\cdot\mathbf{u}_j)^2}{1+\chi'(\mathbf{u}_i\cdot\mathbf{u}_j)} + \frac{(\hat{\mathbf{r}}_{ij}\cdot\mathbf{u}_i - \hat{\mathbf{r}}_{ij}\cdot\mathbf{u}_j)^2}{1-\chi'(\mathbf{u}_i\cdot\mathbf{u}_j)}\right], \tag{6}$$

$\chi=(\kappa^2-1)/(\kappa^2+1)$ and $\chi'=[(\kappa')^{1/\nu'}-1]/[(\kappa')^{1/\nu'}+1]$. As in the original paper (Ref. 5), we choose $\nu'=2$ and $\nu=1$. We also set $\kappa'=5$, allowing different values for the geometrical anisotropy between $\kappa=3$ and 4.

The dipolar potential energy U_{ij}^{dd} between two molecules is given by

$$U_{ij}^{dd} = \frac{\mu^2}{r_d^3}\left(\mathbf{u}_i\cdot\mathbf{u}_j - \frac{3(\mathbf{u}_i\cdot\mathbf{r}_d)(\mathbf{u}_j\cdot\mathbf{r}_d)}{r_d^2}\right), \tag{7}$$

where $\mathbf{r}_d=\mathbf{r}_{ij}+d(\mathbf{u}_j-\mathbf{u}_i)$ is the vector joining the two point dipoles and μ is the dipolar moment of the molecule.

The dipolar GB pair potential $U_{ij}=U_{ij}^{\mathrm{GB}}+U_{ij}^{dd}$ energy contours for $\kappa=3$, $\mu=2\sqrt{\epsilon_0\sigma_0^3}$, and $d=\sigma_0$ are represented in Fig. 1 for parallel and antiparallel configurations. Note that they are the relevant configurations for orientationally ordered phases. For the antiparallel case, two different local minima are observed: the global minimum associated mainly with the presence of the dipole at roughly $\theta\approx 18°$ ($U_{ij}\approx -10.7\epsilon_0$), where θ is the angle between $\mathbf{r}_{ij}$ and the molecular orientation of the central particle $\mathbf{u}_i$. Additionally there is a

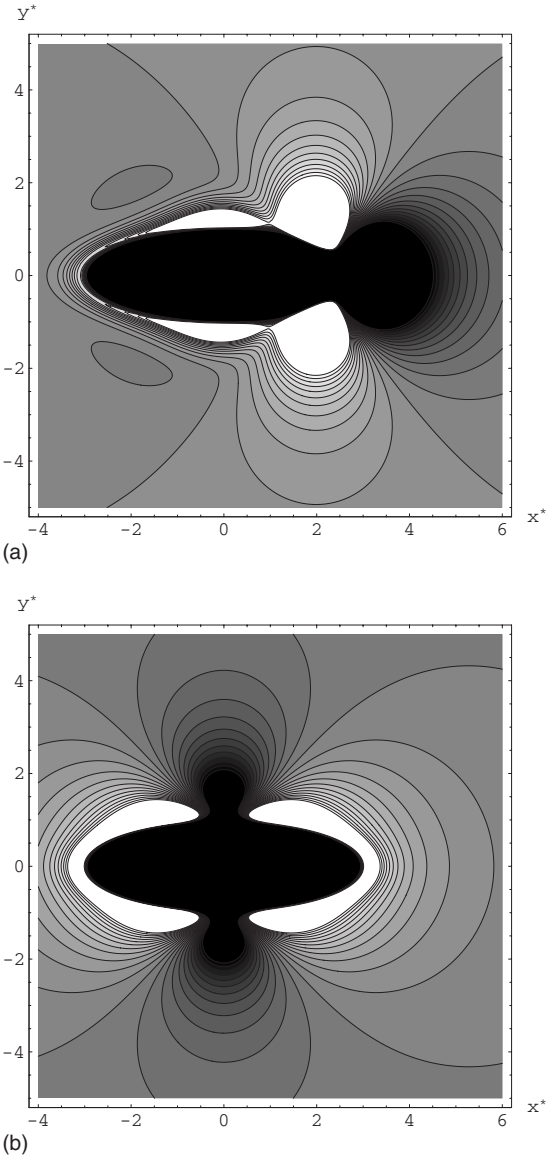

FIG. 1. Potential energy contours of the dipolar GB pair potential between a particle placed at the origin and its molecular axis oriented along the $x>0$ semiaxis, and another particle placed in an arbitrary position on the $z=0$ plane and oriented parallel (top) and antiparallel (bottom) with respect to the particle at the origin. Lighter shadowing represents lower energies. The potential parameters are $\kappa=3$, $\kappa'=5$, $\mu=2\sqrt{\epsilon\sigma_0^3}$, and $d=\sigma_0$ (see text for explanation).

local minimum associated with the GB part of the potential at $\theta\approx 85°$ ($U_{ij}\approx -1.3\epsilon_0$). Finally, the effective hard-body shape corresponding to this configuration, estimated from the $U_{ij}=0$ contour, has a pearlike shape, which may also lead to the formation of interdigitated bilayered smectic phases.[30] For the parallel configuration, two equivalent minima are obtained for $\theta\approx 40°$ and $\theta\approx 140°$ ($U_{ij}\approx -1.6\epsilon_0$). The repulsive part of the potential is swollen in the equatorial zone of the GB molecule due to the presence of the dipole, although the dipolar repulsion is softer than the induced by the GB potential ($U_{ij}=4\epsilon_0$ for $\theta=90°$ and $r_{ij}=\sigma_0$).

Following the same strategy used to study nonpolar GB and central dipolar GB model,[2–4] we carry out Monte Carlo computer simulations in the isothermal-isobaric ensemble (NPTMC). Our simulations are performed for $N=1372$ par-

TABLE I. Thermodynamic and structural properties of the terminal dipolar GB model with $\kappa=3$ and $\mu^*=2$. T^* and p^* are the reduced temperature and pressure, $\rho^*=\rho\sigma_0^3$ is the reduced number density, $u^*=U/N\epsilon_0$ is the reduced potential energy per particle, S is the nematic order parameter, and B_4 is the tetragonal bond-orientational order. For each state, we identify the corresponding phase (see text for explanation).

T^*	p^*	ρ^*	u^*	S	B_4	Phase
0.50	0.1	0.3352(6)	−15.989(14)	0.9900(4)	0.856(7)	SmT_d
0.50	0.5	0.3425(5)	−16.085(11)	0.9905(4)	0.858(6)	SmT_d
0.50	1.0	0.3503(4)	−16.155(15)	0.9911(4)	0.857(6)	SmT_d
0.50	2.0	0.3618(4)	−16.199(8)	0.9909(5)	0.863(6)	SmT_d
0.50	3.0	0.3748(8)	−16.223(12)	0.9907(3)	0.874(4)	SmT_d
0.50	4.0	0.3825(4)	−16.187(13)	0.9909(4)	0.866(3)	SmT_d
0.50	5.0	0.3891(3)	−16.101(13)	0.9906(3)	0.859(4)	SmT_d
0.50	6.0	0.3953(3)	−16.042(14)	0.9916(3)	0.867(3)	SmT_d
0.50	7.0	0.4070(6)	−16.07(3)	0.9903(9)	0.897(5)	SmT_d
0.50	8.0	0.4108(3)	−15.998(14)	0.9927(5)	0.898(3)	SmT_d
1.00	0.1	0.2897(19)	−13.61(7)	0.960(2)	0.512(19)	SmT_d
1.00	0.5	0.3203(15)	−14.24(5)	0.9677(13)	0.745(16)	SmT_d
1.00	4.0	0.3811(6)	−15.00(3)	0.9551(16)	0.825(5)	SmT_d
1.00	7.0	0.3996(5)	−14.91(2)	0.9561(13)	0.815(6)	SmT_d
1.25	0.1	0.0875(17)	−3.11(7)	0.029(9)	⋯	I
1.25	0.5	0.2845(17)	−12.00(9)	0.937(3)	0.073(13)	SmA_d
1.25	1.0	0.3276(13)	−13.51(5)	0.9660(11)	0.550(13)	SmT_d
1.25	7.0	0.4025(6)	−14.93(3)	0.9757(19)	0.905(4)	SmT_d
1.50	1.0	0.21115(13)	−4.834(8)	0.04(4)	⋯	I
1.50	1.5	0.294(2)	−11.17(14)	0.914(6)	0.071(31)	SmA_d
1.50	2.0	0.3328(17)	−12.89(7)	0.958(2)	0.672(19)	SmT_d
1.50	3.0	0.3556(13)	−13.59(5)	0.968(2)	0.792(11)	SmT_d
1.50	5.0	0.3794(9)	−14.15(4)	0.968(3)	0.857(8)	SmT_d
1.50	7.0	0.3944(7)	−14.34(4)	0.9715(17)	0.878(5)	SmT_d
2.00	4.0	0.2745(11)	−4.83(7)	0.06(2)	⋯	I
2.00	4.5	0.351(2)	−12.51(12)	0.965(3)	0.748(27)	SmT_d
2.00	5.0	0.3555(15)	−12.57(8)	0.963(2)	0.740(13)	SmT_d
2.00	6.0	0.3680(11)	−12.92(5)	0.9693(15)	0.785(10)	SmT_d
2.50	7.0	0.2968(10)	−4.02(7)	0.057(16)	⋯	I
2.50	8.0	0.3069(10)	−4.05(7)	0.065(16)	⋯	I
2.50	9.0	0.3691(15)	−11.33(14)	0.947(5)	0.690(17)	SmT_d
2.50	10.0	0.3865(10)	−12.48(7)	0.9777(10)	0.845(7)	SmT_d
3.00	10.0	0.3101(9)	−3.09(6)	0.05(2)	⋯	I
3.00	11.0	0.3184(11)	−3.10(8)	0.11(5)	⋯	I
3.00	12.0	0.3266(11)	−3.16(10)	0.19(7)	⋯	I
3.00	13.0	0.03432(10)	−3.94(8)	0.656(18)	⋯	N
3.00	14.0	0.3507(12)	−4.00(10)	0.69(2)	⋯	N
3.00	15.0	0.3898(12)	−10.16(16)	0.949(4)	0.686(15)	SmT_d
3.00	16.0	0.3977(11)	−10.73(14)	0.961(4)	0.744(11)	SmT_d
3.50	13.0	0.3200(8)	−2.17(6)	0.061(17)	⋯	I
3.50	14.0	0.3262(9)	−2.10(6)	0.060(11)	⋯	I
3.50	15.0	0.3345(10)	−2.13(7)	0.22(2)	⋯	I
3.50	16.0	0.345(2)	−2.55(9)	0.51(3)	⋯	N
3.50	17.0	0.353(3)	−2.65(9)	0.61(4)	⋯	N
3.50	18.0	0.361(3)	−2.75(8)	0.72(4)	⋯	N
3.50	19.0	0.367(4)	−2.73(7)	0.72(4)	⋯	N
3.50	20.0	0.3722(11)	−2.77(8)	0.77(4)	⋯	N
3.50	21.0	0.3758(9)	−2.72(9)	0.766(10)	⋯	N
3.50	22.0	0.3801(8)	−2.65(9)	0.781(11)	⋯	N
3.50	23.0	0.4121(9)	−9.09(13)	0.959(2)	0.708(10)	SmT_d
3.50	24.0	0.4166(9)	−9.26(15)	0.966(3)	0.734(13)	SmT_d
3.50	25.0	0.4201(8)	−9.32(12)	0.9685(18)	0.745(10)	SmT_d
4.00	18.0	0.3374(9)	−1.04(8)	0.09(6)	⋯	I
4.00	19.0	0.3447(11)	−1.10(10)	0.25(5)	⋯	I
4.00	20.0	0.3563(12)	−1.60(10)	0.60(3)	⋯	N
4.00	21.0	0.3637(15)	−1.74(12)	0.67(3)	⋯	N
4.00	22.0	0.3678(10)	−1.62(9)	0.692(18)	⋯	N

TABLE I. (*Continued.*)

T^*	p^*	ρ^*	u^*	S	B_4	Phase
4.00	23.0	0.3724(11)	−1.57(10)	0.713(18)	⋯	*N*
4.00	24.0	0.3764(13)	−1.51(10)	0.75(2)	⋯	*N*
4.00	25.0	0.3810(9)	−1.43(9)	0.750(12)	⋯	*N*
4.00	26.0	0.3858(11)	−1.37(8)	0.77(2)	⋯	*N*
4.00	27.0	0.3895(15)	−1.20(11)	0.78(4)	⋯	*N*
4.00	28.0	0.393(3)	−1.15(11)	0.79(3)	⋯	*N*
4.00	29.0	0.396(3)	−1.05(12)	0.80(2)	⋯	*N*
4.00	30.0	0.399(3)	−0.96(17)	0.81(2)	⋯	*N*
4.00	31.0	0.403(4)	−0.8(2)	0.826(19)	⋯	*N*

ticles. The reaction field method with a dielectric constant $\epsilon_{\mathrm{RF}}=\infty$ and a cutoff $R_c^{\mathrm{RF}}=4\sigma_0$ ($\kappa=3$) and $R_c^{\mathrm{RF}}=6\sigma_0$ ($\kappa=4$) has been used to deal with the long-range character of the dipolar interactions (for details of the simulations, see the Refs. 2, 19, 28, 29, 31, and 32). Each MC cycle consisted of N attempted particle translations and rotations and one volume change, where the three dimensions of the box were allowed to change independently. This procedure is particularly helpful when smectic phases appear in the simulations. In addition, an attempted dipole flip was randomly done with a 25% frequency compared to the 75% of the conventional translation-rotational moves to prevent locking in metastable states.

The simulation procedure is the following. The simulation for the lowest pressure of each isotherm starts from a configuration at a very low density of particles ($\rho^*\equiv\rho\sigma_0^3=0.01$) and a random molecular orientation distribution. Each simulation takes as initial configuration the final output of the previous simulation at lower pressure. The number of cycles for each simulation is of order of 2×10^5 for disordered phases and up to 3×10^6 cycles long for spacially ordered phases. After a period of equilibration (longer for orientationally ordered systems than for isotropic systems) a set of physical quantities, such as the average energy U and density $\rho=N/\langle V\rangle$, as well as their statistical errors, are evaluated from the remainder of the run. The orientational order is characterized by the nematic order parameter S, defined as the largest eigenvalue of the order tensor Q,

$$Q=\left\langle \frac{1}{N}\sum_{i=1}^{N}\frac{3\mathbf{u}_i\otimes\mathbf{u}_i-I}{2}\right\rangle. \tag{8}$$

Additionally the orientational ordering of the molecular dipoles is also monitorized by the global polarity P_1,

$$P_1=\left\langle \frac{1}{N}\left|\sum_{i=1}^{N}\mathbf{u}_i\cdot\mathbf{n}\right|\right\rangle, \tag{9}$$

where $\mathbf{n}$ is the nematic director defined as the eigenvector of Q associated with its largest eigenvalue S.

In order to characterize the microscopic structure, we evaluate a series of correlation functions. The first and second orientational correlation functions $g_1(r)$ and $g_2(r)$ are defined as

$$g_i(r)=\frac{\langle\Sigma_i\Sigma_{j\neq i}\delta(r-r_{ij})P_i(\mathbf{u}_i\cdot\mathbf{u}_j)\rangle}{\langle\Sigma_i\Sigma_{j\neq i}\delta(r-r_{ij})\rangle}\equiv\frac{\langle V\rangle}{4\pi r^2N^2g(r)}\left\langle\sum_i\sum_{j\neq i}\delta(r-r_{ij})P_i(\mathbf{u}_i\cdot\mathbf{u}_j)\right\rangle, \tag{10}$$

where $P_i(x)$ is the ith-order Legendre polynomial ($i=1,2$) and $g(r)$ is the usual pair correlation function. In order to observe the formation of layers in the smectic (or crystalline) phases, we can split the pair distribution function into the pair correlation functions $g_\parallel(r_\parallel)$ and $g_\perp(r_\perp)$, which account for the correlations between the positions of two particles along a direction parallel or perpendicular to the nematic director, respectively. Here the distance $r_\parallel$ is the projection of $\mathbf{r}_{ij}$ along the nematic director $\mathbf{n}$ and $r_\perp$ is the projection onto the plane perpendicular to $\mathbf{n}$. As we anticipate that dipolar correlations will be helpful to understand our results, so we have also evaluated the correlation functions mentioned previously, but referring the position of the molecule not to the center of mass of the molecule, but to the position of the point dipole [$g_\perp^d(r_\perp)$ and $g_\parallel^d(r_\parallel)$].

An alternative way to describe the positional ordering in layered phases is by the evaluation of the density profiles for the molecule centers of mass along the nematic director direction,

$$\rho(z)\equiv\left\langle\sum_{i=1}^{N}\delta(z_i-z)\right\rangle, \tag{11}$$

where z is the position along the nematic director $\mathbf{n}$ and $z_i=\mathbf{r}_i\cdot\mathbf{n}$. In order to see the dipolar ordering, we calculate the analog of the density profile for the dipolar centers $\rho^d(z)\equiv\langle\Sigma_{i=1}^N\delta(z_i^d-z)\rangle$ and the polarity profile $p(z)\equiv\langle\Sigma_{i=1}^N(\mathbf{u}_i\cdot\mathbf{n})\delta(z_i^d-z)\rangle$, where $z_i^d=z_i+d(\mathbf{u}_i\cdot\mathbf{n})$.

The correlation functions mentioned above allow to distinguish between spacially homogeneous and stratified phases. However, these functions alone cannot unequivocally determine the nature of the layered phases. To characterize the structure of stratified phases, a bond-orientational order parameter B_ν within the layers has been evaluated. This function is defined as

$$B_\nu=\frac{1}{\nu N}\left\|\left\langle\sum_{j=1}^{N}\sum_{k=1}^{\nu}\exp(i\nu\phi_{jk})\right\rangle\right\|, \tag{12}$$

where ϕ_{jk} is the angle between the bond linking particles j and k and a fixed reference axis and ν is the number of

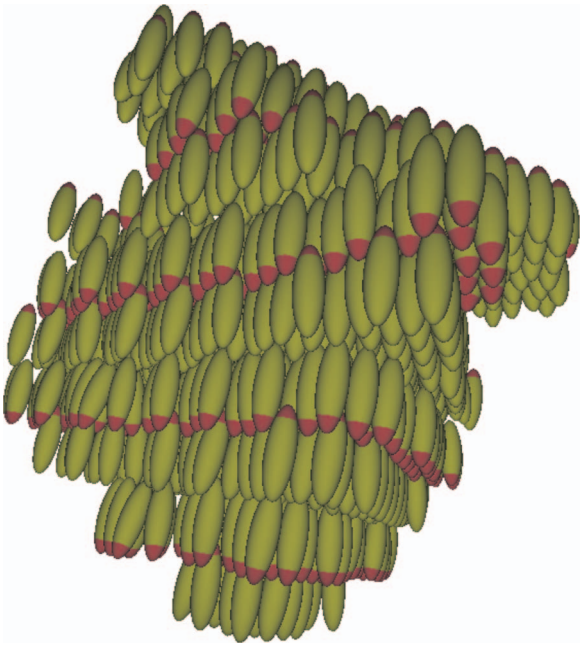

FIG. 2. (Color) Snapshot of 1372 dipolar GB molecules ($\kappa=3, \mu^*=2$) at $T^*=0.5$ and $p^*=0.1$, corresponding to a SmT_d phase. The dipole position along the molecular axis is represented by the color change in the molecule.

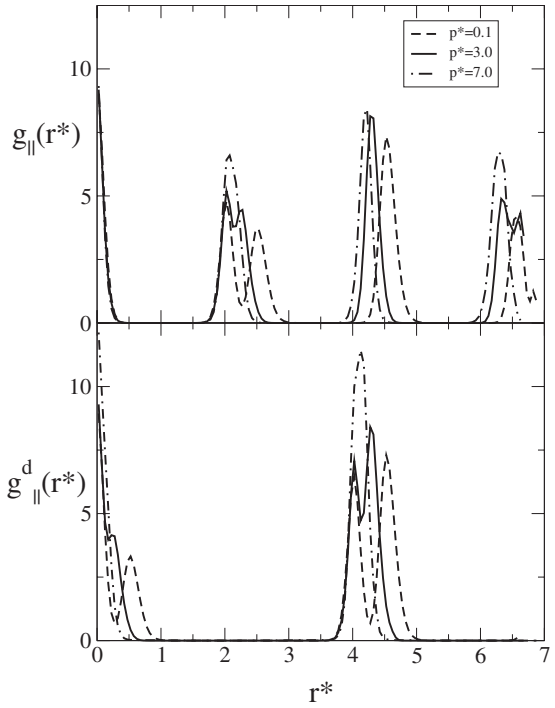

FIG. 3. Plot of the longitudinal pair distribution functions of centers of masses $g_{\|}(r^*)$ (upper panel) and the dipolar centers $g_{\|}^d(r^*)$ (lower panel) for a dipolar GB model with $\kappa=3$ and $\mu^*=2$ at $T^*=0.5$ and different pressures: $p^*=0.1$ (dashed line), $p^*=3.0$ (continuous line), and $p^*=7.0$ (dot-dashed line).

nearest-neighbor bonds, defined as the number of particles to be within $r_b \approx 1.2\sigma_0$ from each one. The parameter ν takes into account the short-range positional order. For example, $\nu=6$ corresponds to a locally hexagonal packing. The order parameter B_ν takes values close to zero when no in-plane orientational bond-order exists and close to one in the presence of perfect in-plane orientational bond order.

III. SIMULATION RESULTS

We have performed computer simulation for GB molecules with a terminal dipole characterized by different geometrical anisotropies κ in a range between $\kappa=3$ and $\kappa=4$. In our study we considered that the dipole is located at a reduced distance $d^* \equiv d/\sigma_0=(\kappa-1)/2$ from the molecular center of mass along the molecular axis, with a reduced dipolar moment strength given by $\mu^* \equiv \sqrt{\mu^2/\epsilon_0\sigma_0^3}=2$.

In the absence of dipole, the phase diagram of the GB model has been previously characterized in the literature.[12] For $\kappa=3$, the only reported phases are the isotropic (I), either vapor or liquid, nematic (N), and smectic-B (SmB) with hexatic in-layer bond orientational. However, there are concerns about the true nature of the SmB phase, which may be a crystal phase.[12] As κ increases, an island of smectic A (SmA) phase appears for $\kappa \geq 3.6$.[12]

When a dipole is placed at the center of mass of the molecule,[2,3] no new phases appear, although it is observed that the presence of the dipolar interactions favors the formation of layered phases. Thus there is a stabilization of the smectic phases with respect to either the isotropic or nematic phase. However, the relative stability between the isotropic and nematic phases is virtually unaffected by the presence of the dipole.

A. $\kappa=3.0$

We have studied the isotherms $T^* \equiv k_B T/\epsilon_0=0.50$, 1.00, 1.25, 1.50, 2.00, 2.50, 3.00, 3.50, and 4.00 (see Table I). Our results show a dramatic change in the phase diagram, confirming that the presence of the dipole stabilizes layered phases with respect to the nematic or isotropic phase. This contrasts with the reported results for hard spherocylinders with a terminal dipole, in which a dramatic stabilization of the nematic phase relative to the smectic phase is observed.[17] For the lower temperatures ($T^*=0.50$ and 1.0), the only observed phase for reduced pressures $p^*=p\sigma_0^3/\epsilon_0$ larger than 0.05 is a layered phase (see snapshot in Fig. 2). Figure 3 plots the correlation functions $g_{\|}(r_{\|})$ and $g_{\|}^d((r_{\|})$ for different pressures. The bilayered character of the phase is revealed by the splitting of the second peak of $g_{\|}$ corresponding to the two neighboring layers. This is confirmed by the analysis of the density and dipolar density profiles (see Fig. 4) and the alternance of the dipolar orientations. The dipoles of the molecules on each layer which composes the bilayer are pointing outward. Examination of $g_{\|}$ shows that the distance between the layers which compose the bilayer is nearly constant and equal to $2\sigma_0 < \kappa\sigma_0$. This indicates a strong interdigitation between them. It was also observed correlation between particles of neighboring layers, which may indicate a solidlike character of the phase. There is also interdigitation between the closest layers corresponding to different neighboring bilayers, but their distances decrease as the pressure is increased. The examination of the dipole densities for different pressures shows that under compression, the dipole layers corresponding to neighboring bilayers coalesce into a single

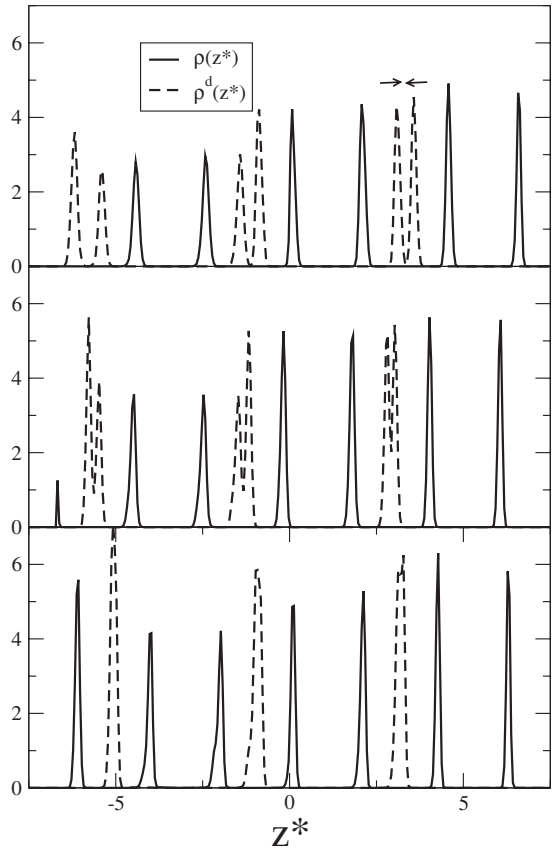

FIG. 4. Center of mass densities $\rho(z^*)$ (continuous lines) and dipolar center densities $\rho^d(z^*)$ (dashed lines) measured along the director for $T^*=0.5$ and different values of the pressure p^*: $p^*=0.1$ (upper panel), $p^*=3.0$ (central panel), and $p^*=7.0$ (lower panel). The geometrical anisotropy parameter is $\kappa=3$, and the arrows represent the dipole orientation at the central peaks.

layer for high enough pressure (see Figs. 3 and 4). We have not been able, however, to check if this structural transition is a signature of the appearance of a new phase.

The phase described above is analogous to the antiferroelectric smectic phase reported by Berardi *et al.*[27–29] for other molecular parameters. In order to fully characterize this phase, we have studied the in-layer positional correlations. The hexatic bond-orientational order B_6 gives negligible values. However, the values of B_4 show that the molecules arrange in each layer in a tetragonal fashion. This positional ordering is also put into manifest by the transversal correlation function $g_\perp$, which shows a significant in-layer structure, and the positions of the maxima are consistent with the location of the nodes of a square lattice. We will denote this interdigitated bilayered antiferroelectric smectic phase with in-layer tetragonal-positional order as the SmT_d phase. This tetragonal in-layer ordering has been also observed in GB models with a terminal dipole for $\kappa=4$ and $d^*=0.5$ (Ref. 33) and with two opposing terminal dipoles.[34] Experimentally this in-layer structure has been observed in ionic liquid crystals.[35,36]

For higher temperatures and the same range of pressures, new phases appear. The isotropic phase is observed for all the temperatures considered above $T^*=1.00$ and small pressures. Upon compression of the system, the isotropic phase

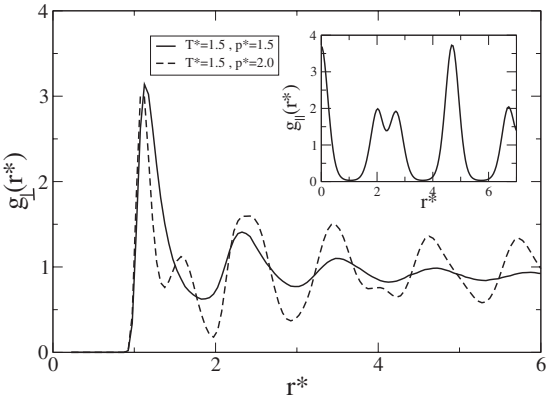

FIG. 5. Transversal pair correlation function $g_\perp(r^*)$ for $T^*=1.5$ and $p^*=1.5$ (continuous line) and $p^*=2.0$ (dashed line). Inset: longitudinal pair correlation function $g_\parallel(r^*)$ for $T^*=1.5$ and $p^*=1.5$. The geometrical anisotropy parameter is $\kappa=3$.

changes to bilayered structures for $T^*=1.25$ and $T^*=1.50$ at $p^*=0.5$ and $p^*=1.5$, respectively. Analysis of the density and dipole profiles, as well as $g_\parallel$, shows a similar interdigitated antiferroelectric stratification to the SmT_d phase. However, the in-layer structure is liquidlike as $B_\nu \approx 0$ for $\nu=4$ and 6. Furthermore, $g_\perp$ shows a liquidlike structure, so we can identify this phase as SmA_d (see Fig. 5). It is worthwhile to note that true SmA was never reported for $\kappa=3$ in the absence or with central dipole. Further pressure increase leads to a transition to the SmT_d phase. The temperature and pressure range at which the SmA_d phase appears is quite limited, and no trace of it appears for $T^* \geq 2$. However, the stability of this phase has been confirmed as it was obtained from both disordered and SmT_d-like configurations.

For $T^* \geq 3.00$ the nematic phase intrudes between the I and SmT_d phases. Again, the late appearance of the nematic phase (in the absence of dipole, it appears for $T^* \geq 0.83$) is a consequence of the stabilization of the smectic phases by the dipolar interaction.

We have heated the system up to $T^*=4.00$. Although for high enough temperatures (or pressures) the SmB phase is expected to appear, no sign of it was observed.

B. $\kappa=4.0$

We consider now the geometrical anisotropy parameter $\kappa=4$. We have done simulations for $T^*=1.50$, $T^*=1.75$, and $T^*=2.00$ (see Table II). For the lowest temperature, we observe only an antiferroelectric and interdigitated bilayered phase (see Fig. 6). However, the in-layer structure differs to the corresponding to the SmT_d phase for $\kappa=3$. Now, for $\nu=4$, B_ν is negligible, but for $\nu=6$ takes nonvanishing values. Consequently, this phase has a hexatic in-layer positional ordering, so we will denote this phase as SmB_d. This is also confirmed by the change in the positions of the maxima observed in the transversal correlation function $g_\perp$ (see Fig. 6 for $T^*=1.5$ and $p^*=1.0$), now consistent with the location of the nodes on a triangular lattice. As the temperature is increased, new phases are observed: an isotropic fluid phase for low densities and a SmA_d phase between the I and the SmB_d phase. The stability range for the SmA_d phase is larger

TABLE II. Thermodynamic and structural properties of the terminal dipolar GB model with $\kappa=4$ and $\mu^*=2$. For each state, we identify the corresponding phase (see text for explanation).

T^*	p^*	ρ^*	u^*	S	B_6	Phase
1.50	0.1	0.2081(18)	−17.51(12)	0.941(5)	0.628(15)	SmB_d
1.50	0.25	0.2170(14)	−17.16(10)	0.963(2)	0.644(17)	SmB_d
1.50	0.5	0.2306(12)	−17.74(10)	0.9723(14)	0.611(16)	SmB_d
1.50	1.0	0.2429(10)	−18.47(8)	0.9775(13)	0.488(16)	SmB_d
1.50	2.0	0.2598(7)	−19.06(7)	0.9840(8)	0.522(11)	SmB_d
1.50	3.0	0.2660(7)	−19.12(7)	0.9845(7)	0.512(10)	SmB_d
1.75	0.25	0.0838(2)	−3.98(4)	0.0365(6)	⋯	I
1.75	0.5	0.2011(13)	−14.90(10)	0.9472(19)	0.037(18)	SmA_d
1.75	0.75	0.2121(12)	−15.51(9)	0.9550(17)	0.058(25)	SmA_d
1.75	1.0	0.2204(13)	−15.95(9)	0.9595(17)	0.062(32)	SmA_d
1.75	1.25	0.2342(14)	−16.98(13)	0.9692(17)	0.512(33)	SmB_d
2.00	0.5	0.1024(11)	−3.68(10)	0.033(10)	⋯	I
2.00	0.75	0.1229(12)	−4.34(10)	0.038(13)	⋯	I
2.00	1.0	0.1988(16)	−13.43(18)	0.925(5)	0.028(17)	SmA_d
2.00	1.25	0.2140(12)	−14.73(10)	0.9481(19)	0.050(25)	SmA_d
2.00	1.5	0.2200(13)	−15.06(11)	0.952(2)	0.054(30)	SmA_d
2.00	1.75	0.2258(11)	−15.39(10)	0.956(2)	0.073(34)	SmA_d
2.00	2.0	0.2315(10)	−15.73(9)	0.9590(16)	0.104(42)	SmA_d
2.00	2.50	0.2468(11)	−17.11(10)	0.9732(14)	0.607(17)	SmB_d

than for $\kappa=3$, as expected since the larger elongation of the molecules favors the formation of the SmA phase, even in the absence of dipole. We do not find any trace of a nematic phase, which should be observed for higher temperatures.

C. From $\kappa=3.0$ to $\kappa=4.0$

In order to understand the appearance of different smectic phases, we have considered the effect of κ on the in-layer structure. Thus we have done simulations for $T^*=0.5$ and $p^*=0.5$, which corresponds to a SmT_d phase for $\kappa=3$ and SmB_d phase for $\kappa=4$, and we have studied different elongations $\kappa=3.1$, $\kappa=3.2$, and $\kappa=3.3$. Our results show that for κ smaller than 3.3, the in-layer structure is always tetragonal, so the equilibrium phase is SmT_d. However, for $\kappa\geq 3.3$, a SmB_d is developed. We have checked the consistency of these results by beginning from different initial conditions. So, Fig. 7 shows the evolution of B_4 and B_6 for $\kappa=3.3$ when the initial condition corresponds to a SmT_d-like configuration. As it can be seen, the tetragonal in-layer structure crossovers to a hexatic one smoothly, indicating that the SmT_d and the SmB_d structures can be transformed in each other by a continuous transformation. On the other hand, we anticipate that for some values of κ between 3 and 4 both SmT_d and SmB_d may coexist. However, the nature of the transition between these two bilayered states is unknown and beyond our present study.

IV. CONCLUSIONS

In this paper we have presented computer simulations of GB molecules with a strong terminal dipole ($\mu^*=2$) placed at $d^*=(\kappa-1)/2$. We have observed that the dipole stabilizes the formation of layered phases with respect to the fluid phases. Their interdigitation and dipolar ordering are similar to that already reported in the literature,[27–29,33] which is a consequence of the interplay between the dipolar interaction

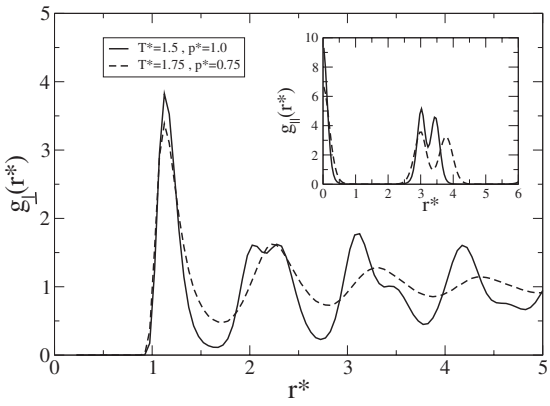

FIG. 6. Transversal pair correlation function $g_\perp(r^*)$ for $T^*=1.5$ and $p^*=1.0$ (continuous line) and $T^*=1.75$ and $p^*=0.75$ (dashed line). The geometrical anisotropy parameter is $\kappa=4$. Inset: longitudinal pair correlation function $g_\parallel(r^*)$ for the same conditions.

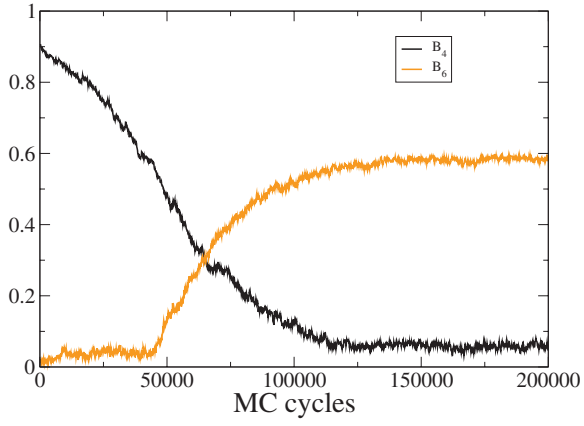

FIG. 7. (Color) Monte Carlo evolution of the bond-order parameters B_4 and B_6 for 1372 dipolar GB molecules with geometrical anisotropy parameter $\kappa=3.3$ at $T^*=0.5$ and $p^*=0.5$. The initial condition corresponds to a SmT_d state.

(controlled by the dipole position and its strength) and the GB interaction (controlled by the geometrical anisotropy κ and the strength of the dispersive interactions). However, we observe *different* layered phases with diverse in-layer molecular organizations. We report the existence of three different antiferroelectric bilayered phases: SmA_d, SmT_d, and SmB_d phases, depending on the geometrical elongation of the molecule. For all these phases, the layers which compose the basic bilayer are at a nearly constant distance smaller than $\kappa\sigma_0$, indicating interdigitation between them. On the other hand, the distance between bilayers increases as the pressure is lowered. For $\kappa=3$ we observe the appearance of a SmA_d and the SmT_d with tetragonal-positional order on the layer. These phases are induced by the presence of an off-centered strong dipole, since no true Sm*A* phase is observed in the absence or with a central dipole. On the other hand, the only layered phase observed without dipole or for a central dipole is a Sm*B* phase, with hexatic in-layer positional order. At this point it is worthy noting that the GB parametrization used by Berardi *et al.*[27–29] (different from ours) allows for the appearance of a Sm*A* phase in the absence of dipole even for $\kappa=3$. As the GB molecule becomes more elongated, the tetragonal in-layer ordering in the SmT_d changes to the more usual hexatic ordering of the SmB_d phase, and for $\kappa=4$ we do not observe the SmT_d phase. For intermediate values of κ both SmB_d and SmT_d phases may coexist. These results show that the molecular geometry plays an important role not only on the onset of the bilayered phases but also in the microscopic organization of the phase.

ACKNOWLEDGMENTS

The authors acknowledge financial support from the Junta de Andalucía (Spain) through Grant No. P06-FQM-01869 and "Ayudas PAIDI FQM-205" and Ministerio de Educación y Ciencia (Spain) through Grant No. ENE2007-68040-C03-02. J.M.R.-E. also acknowledges a "Ramón y Cajal" Fellowship.

[1] M. Born, Sist. Phys. Math. **26**, 614 (1916); Ann. Phys. **55**, 221 (1918).
[2] M. Houssa, A. Oualid, and L. F. Rull, Mol. Phys. **94**, 439 (1998).
[3] M. Houssa, L. F. Rull, and S. C. McGrother, J. Chem. Phys. **109**, 9529 (1998).
[4] M. Houssa, S. C. McGrother, and L. F. Rull, Int. J. Mod. Phys. C **10**, 391 (1999).
[5] J. G. Gay and B. J. Berne, J. Chem. Phys. **74**, 3316 (1981).
[6] E. Velasco, A. M. Somoza, and L. Mederos, J. Chem. Phys. **102**, 8107 (1995).
[7] E. Velasco and L. Mederos, J. Chem. Phys. **109**, 2361 (1998).
[8] E. de Miguel, L. F. Rull, M. K. Chalam, and K. E. Gubbins, Mol. Phys. **74**, 405 (1991).
[9] E. de Miguel, L. F. Rull, and K. E. Gubbins, Phys. Rev. A **45**, 3813 (1992).
[10] L. F. Rull, Physica A **220**, 113 (1995).
[11] E. de Miguel, E. M. del Rio, J. T. Brown, and M. P. Allen, J. Chem. Phys. **105**, 4234 (1996).
[12] J. T. Brown, M. P. Allen, E. M. del Rio, and E. de Miguel, Phys. Rev. E **57**, 6685 (1998).
[13] E. de Miguel and C. Vega, J. Chem. Phys. **117**, 6313 (2002).
[14] J. J. Weis, D. Levesque, and G. J. Zarragoicoechea, Phys. Rev. Lett. **69**, 913 (1992).
[15] D. Levesque, J. J. Weis, and G. J. Zarragoicoechea, Phys. Rev. E **47**, 496 (1993).
[16] J. J. Weis, D. Levesque, and G. J. Zarragoicoechea, Mol. Phys. **80**, 1077 (1993).
[17] S. C. McGrother, A. Gil-Villegas, and G. Jackson, J. Phys.: Condens. Matter **8**, 9649 (1996).
[18] S. C. McGrother and G. Jackson, Phys. Rev. Lett. **76**, 4183 (1996).
[19] A. Gil-Villegas, S. C. McGrother, and G. Jackson, Mol. Phys. **92**, 723 (1997).
[20] A. Gil-Villegas, S. C. McGrother, and G. Jackson, Chem. Phys. Lett. **269**, 441 (1997).
[21] S. C. McGrother, A. Gil-Villegas, and G. Jackson, Mol. Phys. **95**, 657 (1998).
[22] A. Gil-Villegas, G. Jackson, and S. C. McGrother, J. Mol. Liq. **76**, 171 (1998).
[23] S. Varga, I. Szalai, J. Liszi, and G. Jackson, J. Chem. Phys. **116**, 9107 (2002).
[24] G. Sigaud, F. Hardouin, and M. F. Achard, Phys. Lett. **72A**, 24 (1979).
[25] G. Sigaud, F. Hardouin, M. F. Achard, and A. M. Levelut, J. Phys. (Paris) **42**, 107 (1981).
[26] F. Hardouin, M. F. Achard, C. Destrade, and N. H. Tinh, J. Phys. (Paris) **45**, 765 (1984).
[27] R. Berardi, S. Orlandi, and C. Zannoni, Chem. Phys. Lett. **261**, 357 (1996).
[28] R. Berardi, S. Orlandi, and C. Zannoni, Int. J. Mod. Phys. C **10**, 477 (1999).
[29] R. Berardi, S. Orlandi, D. J. Photinos, A. G. Vanakaras, and C. Zannoni, Phys. Chem. Chem. Phys. **4**, 770 (2002).
[30] F. Barmes, M. Ricci, C. Zannoni, and D. J. Cleaver, Phys. Rev. E **68**, 021708 (2003).
[31] J. A. Barker and R. O. Watts, Mol. Phys. **26**, 789 (1973).
[32] B. Garzón, S. Lago, and C. Vega, Chem. Phys. Lett. **231**, 366 (1994).
[33] W. Józefowicz and L. Longa, Phys. Rev. E **76**, 011701 (2007).
[34] R. Berardi, S. Orlandi, and C. Zannoni, Phys. Rev. E **67**, 041708 (2003).
[35] E. Alami, H. Levy, R. Zara, P. Weber, and A. Skoulios, Liq. Cryst. **13**, 201 (1993).
[36] K. Ohta, T. Sugiyama, and T. Nogami, J. Mater. Chem. **10**, 613 (2000).